Nano Energy 115 (2023) 108697

Contents lists available at ScienceDirect

Nano Energy

journal homepage: www.elsevier.com/locate/nanoen

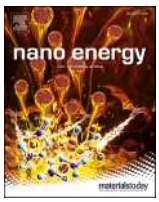

4D printed shape memory metamaterials with sensing capability derived from the origami concept

Wei Zhao [a,1], Nan Li [a,1], Xu Liu [a], Liwu Liu [a], Chengbin Yue [a], Chengjun Zeng [a], Yanju Liu [a,*], Jinsong Leng [b,*]

[a] Department of Astronautical Science and Mechanics, Harbin Institute of Technology (HIT), P.O. Box 301, No. 92 West Dazhi Street, Harbin 150001, People's Republic of China

[b] Center for Composite Materials and Structures, Harbin Institute of Technology (HIT), P.O. Box 3011, No. 2 YiKuang Street, Harbin 150080, People's Republic of China

ARTICLE INFO

Keywords:
4D printing
Shape memory
Mechanical metamaterials
Programmable
Energy harvesting

ABSTRACT

Mechanical metamaterials have unprecedented properties that contribute to the development of science and technology. However, once the mechanical metamaterials are fabricated, the single configuration will limit their application, especially in areas requiring rich programmability and efficient shape reconfigurability, etc. To break through this limitation and explore more potential of mechanical metamaterials, this work proposes a novel design strategy for 4D printed metamaterials with programmable stiffness. Deriving from the origami concept, the stiffness of the structure can be adjusted not only by changing the geometric parameters but also by changing the geometric configuration utilizing the shape memory property. Through numerical simulation, theoretical analysis and experimental tests, the design strategy is verified in the 4D printed mechanical metamaterials. With this strategy, the stiffness of the structure can be adjusted, and the mechanical programmability, shape reconfigurability and adaptability can be significantly improved. Utilizing excellent energy absorption performance, we design and fabricate a kind of shoe sole. By integrating the sensor function of the Triboelectric Nanogenerator (TENG) into the sole, gait monitoring is successfully realized. The 4D printed shape memory metamaterials show extraordinary potential in the field of programmable shock absorption and intelligent monitoring.

1. Introduction

To achieve supernormal mechanical properties, it is usually to design specific artificial microstructural units in three-dimensional space, and the resulting structure is generally called metamaterials [1–6]. Mechanical metamaterials can achieve many different supernormal properties, including lightweight and high strength, adjustable stiffness, negative compressibility, negative Poisson's ratio and bistable [7–10]. The unusual properties are limited by their constituent materials but mainly depend on their micro-structural units and spatial combinations, which can be designed according to the performance requirements [11–14]. The design idea of mechanical metamaterials opens up a new way for the research and development of new structures and shows great potential in sensors [15–17], energy absorption structures[18–20], and reconfigurable antennas[21,22], etc.

Through periodic or aperiodic geometric optimization design of modular units, metamaterials with various mechanical properties can be obtained, which can be freely selected and adjusted according to the requirements[23,24]. Origami, as an ancient art, has been deeply involved in the field of science and engineering[5,24,25]. Origami structure is rich in forms, and many of them have metamaterial characteristics, which can transform the folding principle of origami into a complex three-dimensional structure design concept to realize various functions [26–33].

By introducing the origami concept, the construction and design of unit-cell can break through the limitations of a single form, and obtain more mechanical metamaterials with special properties [34–36]. By geometric design, the origami-derived stacked metamaterials can obtain self-locking characteristics[28], adjustable stiffness[2], and quasi-zero stiffness characteristics[28], which can be used in the field of shock energy dissipation. For a fold pattern, in addition to the manufacturing materials, the mechanical properties are mainly determined by the

* Corresponding authors.
E-mail addresses: yj_liu@hit.edu.cn (Y. Liu), lengjs@hit.edu.cn (J. Leng).
[1] These authors contributed equally

https://doi.org/10.1016/j.nanoen.2023.108697
Received 25 April 2023; Received in revised form 5 June 2023; Accepted 11 July 2023
Available online 13 July 2023

geometric parameters, so the consistency of repeated elements results in the single mechanical properties. However, there are certain circumstances in which structures with gradual stiffness and programmable performance are more appropriate. For example, regarding the car body design, the variable stiffness structure will gradually improve the structural bearing capacity, to protect vehicle occupants from re-injury due to extrusion.

With the development of the Internet of Things technology, electromechanical systems have presented a broad application prospect in the fields of human health, infrastructure and military environmental monitoring. It has the development trend of integration, intelligent function and wireless mobility [37,38], so the energy supply is particularly prominent. Using conventional batteries to power an entire network is expensive to maintain, difficult to recycle and polluting to the environment. One possible alternative method is to capture the energy in the environment. Triboelectric Nanogenerator (TENG) [39–42] was invented by Wang Zhonglin's team in 2012. It is a nano energy technology based on the coupling effect of mechanical interface triboelectrification and electrostatic induction. When two materials with different abilities to gain and lose electrons come into contact, their surfaces will generate equal amounts of positive and negative charges due to friction. When the two materials are separated under the action of load, the positive and negative electrostatic charges are separated in space, and the induced potential difference is generated on the upper and lower surface electrodes. When there is a short circuit between the two electrodes or a load in an external circuit, the induced potential difference will drive the flow of electrons between the two electrodes, resulting in a current. Based on the self-powered performance of the TENG, it can be used as a sensing device or connected with other sensors to monitor gait. For example, Kim et al. [43] designed a kind of Covalent Organic Frameworks-based TENG and integrated them into the hand-strengthening device for exercise monitoring, showing excellent results. Furthermore, Kim et al. [37] fabricated a multi-axis pressure sensor with temperature compensation using additive manufacturing technology, which was integrated into shoes for human motion monitoring and force sensing, opening up a wide range of applications.

In this work, we design a series of origami-derived mechanical metamaterials with different topological parameters, which exhibit excellent mechanical properties. Further, by combining structures with different topological parameters, structures with gradient stiffness are obtained. We fabricate the mechanical metamaterials by 4D printing technology and shape memory polymer [44–47]. The 4D printed origami metamaterials can change their configuration and stiffness by utilizing the shape memory effect (SME), which is different from most origami-derived metamaterials. It breaks through the limitation that the mechanical properties and geometrical configuration of metamaterials can not be changed once they are fabricated. On the basis of studying the energy absorption characteristics of the origami mechanical metamaterials, we select one of the representative structures to explore its application in the sole. Furthermore, the metamaterial structure-based triboelectric nanogenerator (MS-TENG) [39–42] is fabricated to monitor gait and realize self-power and self-sensing.

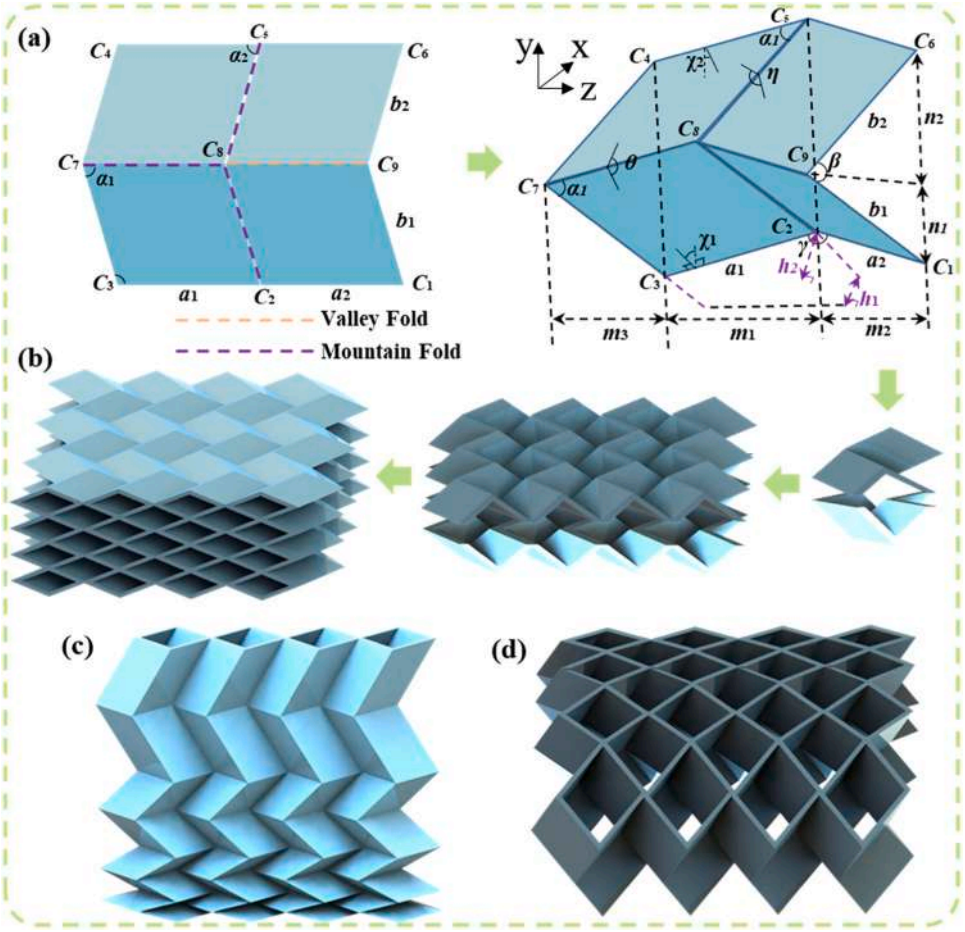

Fig. 1. Parameter definition and structural design of Miura-ori metamaterials (a) Geometric parameter definition of Miura-ori metamaterial (b) Assembly of Miura-ori metamaterials (c) Parametric design of in-plane gradient metamaterials (d) Parametric design of out-of-plane gradient metamaterials.

2. Results and Discussion

2.1. Structure design of Miura-ori metamaterials

How to achieve performance programmability through appropriate geometric topology design and create artificial material structures with unconventional properties is an ongoing challenge. Miura-ori structures are origami patterns formed by a Mosaic arrangement of repeated units, the basic unit of which is shown in Fig. 1(a). It is composed of four identical parallelograms, so its basic shape can be determined by the length of the side a_1, a_2, b_1, b_2, and Angle α_1 and α_2. Generally, unit cells with different topological angles exhibit different mechanical properties.

By extending the unit cell along the X direction, it can be found that two adjacent Miura-ori units share the same parameters including side length a_1 and a_2 and side Angle γ. Changing the topological Angle α_1 can obtain the in-plane gradient structure. Miura-ori structure can complete the continuous superposition along the Z direction by mirroring. In the connection process, different layers are connected by the same parameters b_1 and b_2, and angles γ. Moreover, the structure can be completely folded and expanded because the whole structure still maintains a single degree of freedom. By extending and assembling the unit cell along X, Y and Z directions, the miura-ori metamaterial structures can be obtained as shown in Fig. 1(b).

The geometry of the element embodies the basic elements of all origami structures-mountain or valley folds, where four edges (pleats) are joined together at a single vertex. The key parameters are the dihedral Angle $\theta \in [0, \pi]$, $\eta \in [0, \pi]$ and angle $\alpha \in [0, \pi/2]$. The length, width, and height of the single cell are m, n and d, respectively. Three parameters remain the same whether folded or not, and they are the lengths of the two creases, a and b, and the angles between the two sides of the unit cell. Therefore, we chose the dihedral angle η as the only freedom degree to characterize the geometrical parameter of the unit cell. During the folding process, the ridges of length, a_1, a_2, b_1, b_2, and the angles α_1 and α_2 between the ridges are constant. Therefore, we select the dihedral Angle θ as the control variable to characterize the ori cell. The geometrical relationship satisfies:

$$\eta = 2sin^{-1}[\ell sin(\theta/2)],\ m_i = a_i\ell_i \tag{1}$$

$$n_i = b_i\hbar_i,\ h_i = a_i\ell_i tan\alpha_i cos(\theta/2) \tag{2}$$

$$\chi_i = \sin^{-1}\left[\ell cos(\theta/2)cos^{-1}\alpha_i\right],\ \sin\alpha_1 sin\chi_1 = \sin\alpha_2 sin\chi_2 \tag{3}$$

where $\hbar_i$ and ℓ_i represent dimensionless width and length, and can be further expressed as $\hbar_i = sin\alpha_i \sin(\theta/2)$ and $\ell_i = \cos\alpha_i(1-\hbar_i^2)^{-1/2}$. In addition, the value range of each Angle is: $\eta \in [0,\pi]$, $\theta \in [0,\pi]$, $\beta \in [0,\alpha_1 + \alpha_2]$,$M' = (m_1 + m_2) \in [a_1 cos\alpha_1 + a_2 cos\alpha_2, a_1 + a_2]$, $\gamma \in [\pi - (\alpha_1 + \alpha_2), \pi]$, $h_i \in [0, a_i]$, $\quad i = 1, 2..$.

It is assumed that the Miura-ori metamaterials are consisting of the same periodic diagonal lattice connected by elastic hinges on the edges. The structure can be evenly expanded on a plane. In the folding process, the rigid surface rotates around the ridge. Miura-ori plates are defined by Miura elements, so their geometric characteristics remain consistent throughout. As the angle η changes, the Angle θ, m, n and $d$varies monotonically. When $\eta = 0$, the Miura-ori unit is in a fully folded state, and when $\eta = \pi$, the Miura-ori unit is in a fully unfolded state. The geometric relation of the unit cell satisfies:

$$\begin{aligned} M &= m_1 + m_2 + m_2 \\ &= a_1 \sin\alpha_1 \frac{\sqrt{1-\left(\ell cos(\theta/2)cos^{-1}\alpha_i\right)^2} + j\sqrt{s^2-\left(\ell cos(\theta/2)cos^{-1}\alpha_i\right)^2}}{\sqrt{1-\sin^2\alpha_1\left(\ell cos(\theta/2)cos^{-1}\alpha_i\right)^2}} + b\cos\left(\frac{\beta}{2}\right) \\ N &= n_1 + n_2 = (b_1 + b_2)\sqrt{1-\sin^2\alpha_1 \sin\ell cos(\theta/2)cos^{-1}\alpha_1} \\ H_i &= a_i\ell_i tan\alpha_i cos(\theta/2) \end{aligned} \tag{4}$$

where $s = \sin\alpha_2/\sin\alpha_1$ and $j = a_2/a_1$.

Miura-ori metamaterials are formed by repeated stacking of unit cell. If the geometric parameters of the unit cells in different layers are different, in and out-of-plane gradient Miura-ori metamaterials can be obtained. However, due to the changing geometric parameters of the Miura-ori gradient structure, it is necessary to constrain the geometric parameters of the unit cell in different layers to ensure the perfect connection between layers. To coordinate the deformation of the structure, the adjacent elements should be guaranteed to have the same side length a and the same side Angle γ, and to ensure the coherence of the panel without affecting its motion. Changing the Angle α does not affect the movement of the structure, but it will affect the mechanical properties of the structure.

In contrast to the existing methods of adjusting stiffness by changing thickness and density, the stiffness of origami structures can be systematically changed through geometric design. The mechanical properties of the unit cells can be regulated by changing the topological parameters (See Supporting Information, S1, Fig. S1-S3). Therefore, by the rational arrangement of the unit cell, we can obtain the homogeneous Miura-ori and gradient Miura-ori metamaterials. By changing the topological parameters of Miura origami, and doing superposition or repetition in different directions of space, a series of origami metamaterials with gradual mechanical properties can be designed (Supporting Information, Fig. S4, S5 and S6). As shown in Fig. 1(c) and (d), the Miura-ori structures are composed of multiple elements embedded in and out of the plane and combined in a certain sequence to form gradient Miura-ori metamaterials.

2.2. Mechanical tests of the Miura-ori metamaterials

If mechanical metamaterials are reconfigured to replace traditional materials with stimulation-responsive materials, they will be able to automatically deform, move and change their structural properties or functions in response to external stimuli (See Movie S-I). Furthermore, they will be endowed with richer functional characteristics, including reconfigurable and programmable, etc. In this work, the Miura-ori metamaterial structures are fabricated by shape memory polymer and 4D printing technology(Details see Supporting Information, Section S4, Fig. S7). The quasi-static compression experiment is conducted to investigate the mechanical properties. The compression rate is set as 2 mm/min to avoid the influence of inertia force and kinetic energy as much as possible. The final compression displacement is selected as about 75% of the overall height of the structures. The structure is crushed in this compression distance, and the load response shows a tendency for a dramatic increase. In addition, the finite element software ABAQUS/explicit is used to simulate the mechanical properties of

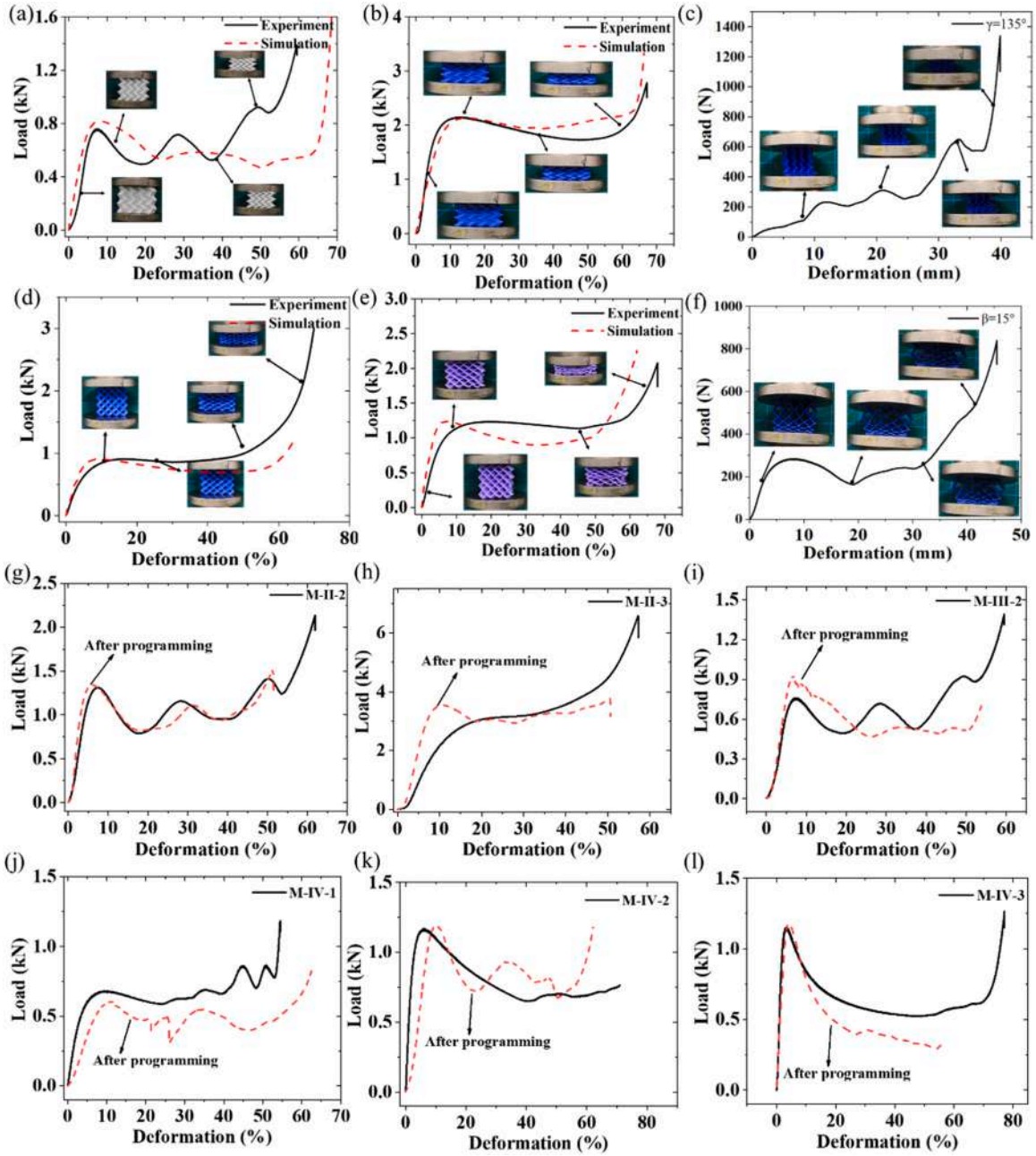

Fig. 2. Mechanical properties testing of Miura-ori metamaterials (a) Mechanical properties of structure M-III-2 under in-plane compression (b) Mechanical properties of structure M-III-3 under in-plane compression (c) Compression performance test of in-plane gradient structures with $\gamma = 135^{\circ}$ (d) Mechanical properties of structure M-III-2 under out-of-plane compression (e) Mechanical properties of structure M-III-3 under out-of-plane compression (f) Compression performance test of out-of-plane gradient structures with $\beta = 15^{\circ}$ Comparison of mechanical properties of metamaterials before and after programming under in-plane compression (g) M-II-2 (h) M-II-3 (i) M-III-2; Comparison of mechanical properties of metamaterials before and after programming under out-of-plane compression (j) M-III-1 (k) M-III-2 (l) M-III-3.

the structures.

Supplementary material related to this article can be found online at doi:10.1016/j.nanoen.2023.108697.

The movement of the structure is mainly rigid rotation around the fold, the smaller the folding Angle, the easier the deformation of the unit. The Mechanical properties testing of structures M-III-2 and M-III-3 under in-plane compression and in-plane gradient structures with $\gamma = 135^{\circ}$ are shown in Fig. 2(a)-(c). The Mechanical properties testing of structures M-III-2 and M-III-3 under out-of-plane compression and in-plane gradient structures with $\beta = 15^{\circ}$ are shown in Fig. 2(d)-(f). For the conventional structure, the compression process can be roughly divided into three stages according to the load-displacement changes and the law of deformation modes. In the first stage, the load increases rapidly to a peak value with the increase of the deformation, which is the elastic deformation stage, and all elements maintain consistent deformation. Subsequently, the displacement continues to increase and the load decreases gradually or remains unchanged until the deformation reaches a certain point, which is the second stage. The mechanical properties of the structure with different topological parameters show obvious differences in this stage. The final stage is the compaction stage, where the load rises sharply with the deformation.

The deformation of the gradual multilayer structure with $\gamma = 135^{\circ}$ presents a step-change rule as shown in Fig. 2(c). The deformation process can roughly be divided into four stages. In the elastic

deformation stage, the deformation ranges from 0 to 2.8 mm, while the load gradually increases and reaches the platform stage, which we label as platform level 1. The Level 1 platform is maintained until the compression displacement is 6.4 mm. The load increases from 111 N to 385 N, when the compression displacement reaches 31 mm, and the gradual stiffness is achieved through structural changes. As exemplified by the structure with $\beta = 15^{\circ}$ as shown in Fig. 2(f), the deformation process can roughly be divided into four stages too. The first is the elastic stage from 0 to 12 mm, and the load increases rapidly to a value and then drops sharply which we label as platform level 1. Subsequently, the deformation of level 2, level 3 and level 4 is 20 mm, 30 mm and 40 mm, respectively.

Based on SME, the shape and mechanical properties of the 4D printed metamaterial can be actively adjusted in a large range and switched between a variety of stable shapes. Consequently, when dealing with extreme external loads, the 4D printed metamaterials can not only protect the object by adjusting the stiffness but also protect themselves from damage. Furthermore, the structure can restore to its original state after deformation and its mechanical properties can be redefined. Fig. 2 (g)-(i) shows the load-deformation curve before and after programming, with good consistency. The angles β of structures M-II-1, M-II-2 and M-II-2 are equal to 120°, 90° and 60°, respectively. By applying a certain deformation to M-II-1, the Angle β can gradually change from 120° to 90°. Similarly, by applying a certain deformation to M-II-2, the Angle β can gradually change from 90° to 60°.

Utilizing SME, heat the 4D printed metamaterials to 90 ℃, and the angles β of M-II-1 and M-II-2 are changed to 90° and 60° by applying a certain displacement, respectively. Subsequently, the configuration is maintained and lowered the temperature to 20 ℃. After this programming process, the configuration of M-II-1 changes to M-II-2, and the configuration of M-II-2 changes to M-II-3. Similarly, this programming approach can be applied to other structures.

Using the same method, the geometrical configuration of the metamaterials along the out-of-plane compression direction can be programmed. The angle γ of Miura-ori metamaterials of M-III series is 90°, while M-IV series is 60°. By applying a certain deformation along the Z-direction, the Angle γ can be changed from 60° to 90°, i.e. the geometrical configuration of the metamaterials of M-III series and M-IV series can switch each other by programming process. To verify whether the programmed structure can show its due mechanical properties under this geometric parameter, we carried out mechanical experiments. The load-displacement curves before and after programming are shown in Fig. 2(j)-(l). The results indicate that the programmed structure has relatively consistent mechanical properties with the original structure. Consequently, it can be concluded that by utilizing SME, not only the structural configuration can be programmed but also the mechanical properties can be re-designed. The 4D-printed metamaterials not only have advantages in the aspects of adjustable stiffness, programmable structure and mechanical properties but also have excellent energy absorption effect (More information can be seen in Supporting Information Fig. S8-S15).

2.3. Schematic of fabrication and working principle

With the development of techniques and the economy, people are paying more and more attention to their daily lives, such as gait monitoring, motion sensing, etc. As smart wearable devices gradually integrate into people's lives, the power supply problem has attracted more and more attention. Self-powered wearable devices can convert mechanical energy into electrical energy to power wearable devices, which has great development prospects. In this work, combined with metamaterials, we develop a kind of 4D printed shoe sole with the ability of self-powered and self-sensing MS-TENG for gait tracking. The design of the sole originated from the Miura-origami method, which could be further programmed, integrated and lightened, as shown in Fig. 3(a). In addition, the MS-TENG can be embedded in normal shoes (Fig. 3(b)), detecting and correcting gaits (Fig. 3(c)) and characterizing different motions (Fig. 3(d)). The flow chart of signal conversions during the self-sensing process is shown in Fig. 3(e).

As a validation, we have designed and fabricated a shoe sole using this metamaterial. For running shoes, efficient energy absorption is an important factor in sole design. They need to be strong enough - not too soft to cause skew - but also have efficient cushioning, energy absorption and shock absorption effect. Exemplified by the metamaterials M-III-2, we design and fabricate a sole with 4D printing technology, and integrate the sensing function to monitor the gait in real-time. Combined with the concept of triboelectric nanogenerators, the metamaterial structure-based triboelectric nanogenerator (MS-TENG) could be designed for converting mechanical energy into electricity. The electrical signals can be used for energy storage and motion monitoring.

PDMS is considered to be one of the triboelectric materials, realizing the combination between piezoelectricity and triboelectricity. The fabrication process of the PDMS-based piezoelectric and flexible thin film (PFF) is shown in Fig. 4(a). The polyvinylidene fluoride (P(VDF-TrFE)), barium titanate (BTO) and polydimethylsiloxane (PDMS) are mixed and cured for 3 h. It is worth noting that part of the BTO content can serve as the nucleating agent of P(VDF-TrFE) to facilitate the formation of the piezoelectric phase-β phase, while the rest of BTO could act as piezoelectric ceramics.

The fabricating diagram of MS-TENG is shown in Fig. 4(b), where the structure M-III-2 with three topological units is chosen to be the substrate. Set one single cell of the structure as an example (the enlarged figure in Fig. 4(b)), the aluminum foil is attached to the dark part to be both the conductive and the positive triboelectric layer. In the opposite

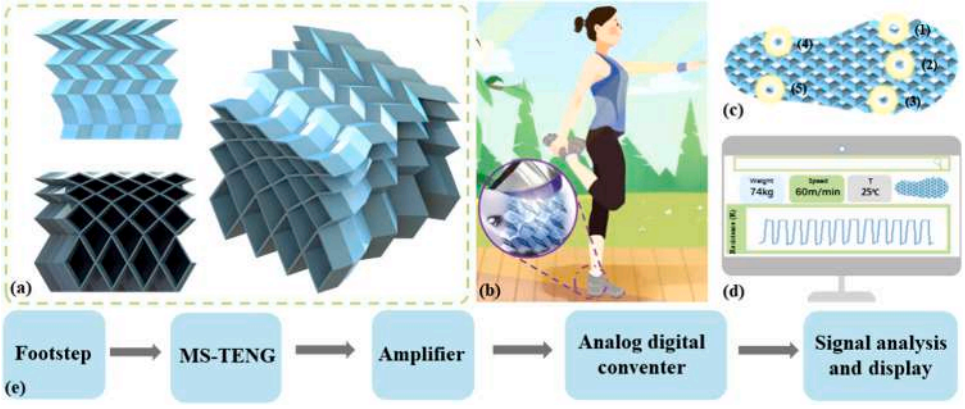

Fig. 3. Schematic illustrations of (a) structure designing (b) application potentials (c), (d) detection of gaits and motions (e) self-sensing flow diagram based on MS-TENG.

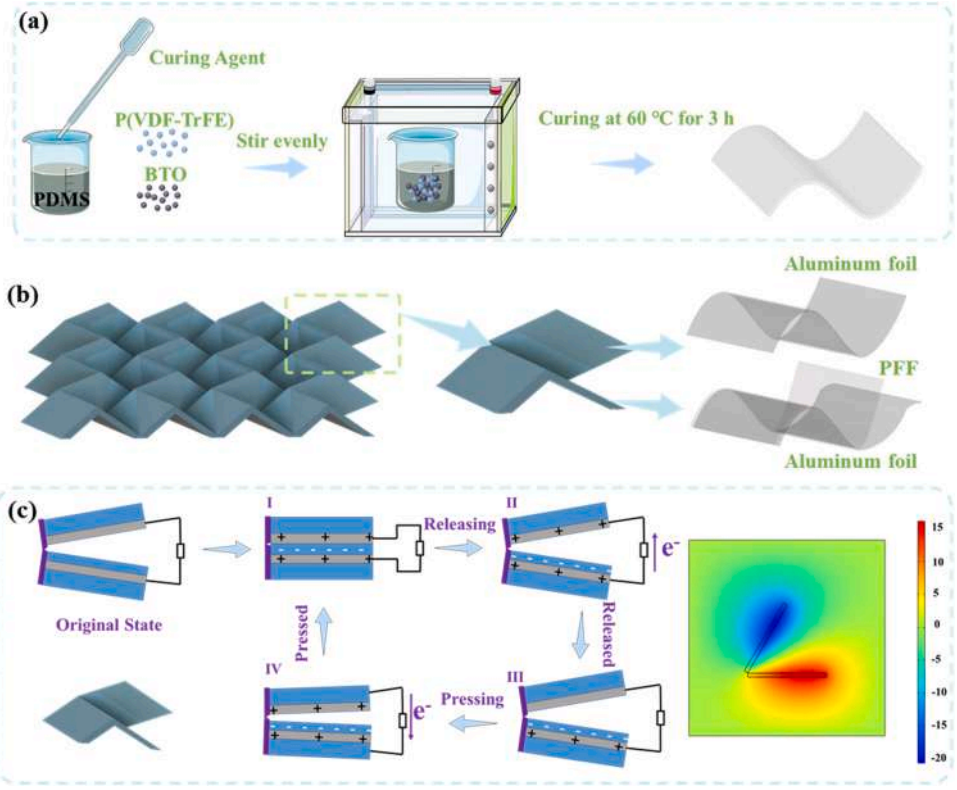

Fig. 4. Schematic diagram of the preparation and fabrication of the MS-TENG (a) Preparation of the piezoelectric and flexible thin film (PFF) (b) Fabrication of the MS-TENG (c) Schematic of the working principle of the MS-TENG (d) Electrical simulation of the MS-TENG via COMSOL.

part, the aluminum foil is pasted first to transfer electrons and the PFF is fixed above serving as the negative triboelectric material. Every two parts form one hybrid nanogenerator, which contributes to the overall MS-TENG.

The working principle of the MS-TENG is shown in Fig. 4(c) which can be classified as the contact-separation modal. In the initial state, both the aluminum and the PFF are in electric neutrality. Once they get in contact with each other, different electrical properties are excited under the attractions of the different nucleus, resulting in the aluminum trend being positive and PFF being negative as shown in Fig. 4(c)-I. During the separating process, the electrical potential changes owing to the distance between the two parts increasing, leading to the transferring of electrons and further the current in external circuits (Fig. 4(c)-II, III). Once the MS-TENG is pressed under external forces, the potential changes again and the electrons flow to the opposite, leading to the reverse current (Fig. 4(c)-IV). At the same time, piezoelectricity triggers once the two parts got in contact, which attributes to the output electrical properties apart from the triboelectricity. The electrical stimulation obtained by COMSOL is shown in Fig. 3, and the trend of potential change is consistent with the experiment and theoretical analysis. The fundamental properties of the film can be seen in Supporting Information Fig. S16-S18.

2.4. Electrical performances of MS-TENG

The fundamental electrical output properties of TENG, PENG and MS-TENG are investigated. The working diagram and testing methods are shown in Fig. 5(a), where the MS-TENG is fixed to the linear motor and tested under different loading values and frequencies. The output currents increase from 0.38 μA to 1.31 μA, simultaneously, the voltages grow from 27.51 V to 89.27 V constantly with frequency increasing from 1 Hz to 5 Hz under 10 N pressure (Fig. 5(b) and (c)). The more frequent the loading is, the faster the potential changes, further to higher currents and voltages. Besides, the relationship between output properties and the loading values is demonstrated under the constant frequency of 4 Hz, as shown in Fig. 5(d) and (e). Both the output voltage and current show increasing trends in loading values (from 5 N to 25 N) and the maximum is 131.3 V and 1.10 μA, respectively. The load value is a key factor for piezoelectric nanogenerators (PENGs), while triboelectric nanogenerators depend on frequencies more. Meanwhile, TENGs are featured with high voltages, while PENGs are characterized more by current (More details can be seen in Supporting Information S8, Fig. S19-S21). As a result, both the values and the frequencies of loading promote the combination between TENGs and PENGs.

In addition, the output voltage shows a linearly related to the applied loading values, and the sensitivity is calculated to be $4.68 \pm 0.6\ V{\cdot}N^{-1}$ (R^2 =0.956) as shown in Fig. 5(d), which indicates the potential in the sensing area. The output voltages under different external load resistance are tested, and the maximum power density is calculated to be 77 nW/cm^2 under 100 MΩ as shown in Fig. 5(f). Considering that stability is essential for the practical application of the MS-TENG, the real-time working cycles test is carried out under 15 N and 10 Hz, as shown in Fig. 5(g) & (h). It is obvious that MS-TENG can output electrical signals steadily under 10,000 cycles, which proves the good robustness under long-time contact and the capability of daily use for motion monitoring.

To verify the energy harvesting effect of the structure, the device is connected to some LEDs that arrange to a "HIT" shape. The circuit diagram and the lighted LEDs are shown in Fig. 6(a) and (b), respectively. All LEDs are successfully lit under the action of cyclic load, which can light up about two hundred LEDs. (Details see in Supporting Information, Movie S-II).

Supplementary material related to this article can be found online at doi:10.1016/j.nanoen.2023.108697.

Trigger unit as a trigger signal generation mode is widely used in industrial production and the Internet of Things as a sensor. If self-powered trigger units can be prepared, it will provide a more energy-

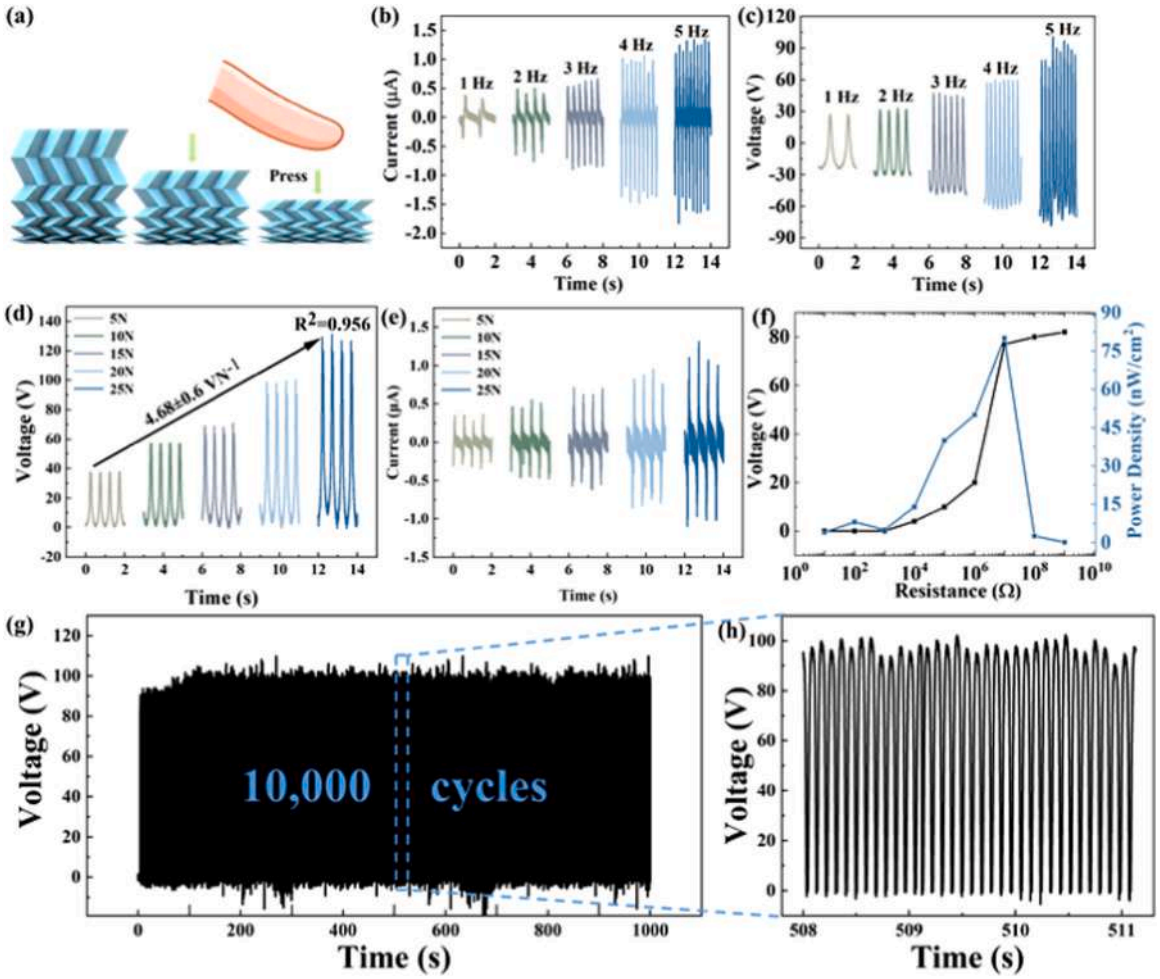

Fig. 5. Basic electrical performance output (a) Loading schematic diagram of the MS-TENG (b), (c) Short-circuit current and open circuit voltage at different loading frequencies (d), (e) Open circuit voltage and short-circuit current and under different pressures (f) Output power under different load resistances (g), (h) Robustness test of open circuit voltage under 10,000 cycles.

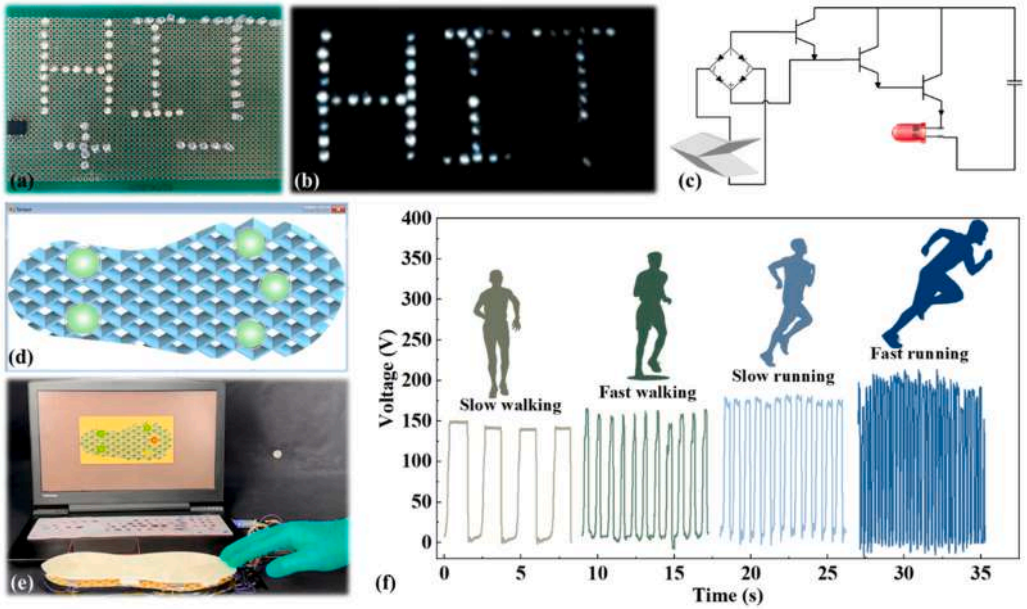

Fig. 6. Functional application of the Miura-ori metamaterials integrating triboelectric-piezoelectric sensing function (a) The arrangement diagram of LEDs (b) The lighted LEDs (c) The equivalent circuit diagram of the self-powered touch switch (d) The arrangement of sensors on the sole (e) Human-computer interaction interface (f) Output characteristics of the human body tested by the triboelectric-piezoelectric sensor.

efficient way of human-computer interaction. In this paper, a simple self-powered touch switch is designed and prepared by combining the three-stage amplifier circuit. The trigger module can be extended to meet the requirement in different application fields. Connect the prepared energy harvesting device to the three-stage amplifying circuit which is used to amplify the electrical signal output as shown in Fig. 6 (c). The signal lamp can blink by pressing the energy harvesting device, the demonstration video can be found in Supporting Information, Movie S-II.

In the field of life medicine, step frequency signals can be used to detect the motion state of patients. The motion state of patients can be obtained by analyzing the electric signals generated by the triboelectric-piezoelectric unit, which has a good early warning function for the pathological characteristics of non-strenuous exercise. At present, most of the step frequency sensors are electronic products, which not only cause high costs but also cause certain damage to the human body due to the radiation effect of electronic products themselves. Consequently, we extend the functionality of the structure as a trigger unit and sensor function and integrate it into the sole to monitor the gait and forces at different positions. The realization of the monitoring function is based on the conversion between mechanical and electrical signals. Voltage data sets of different actions are collected through the response mechanism of mechanical compression and voltage signal. In this work, the triboelectric-piezoelectric unit generates electrical signals by taking advantage of the difference between the gain and loss of electronic capabilities of the two materials. The materials selected in this paper, such as PDMS and Al, have no damage to the human body. Their thickness is extremely thin, their plasticity is in line with human characteristics, and they are comfortable to wear. The possible physiological characteristics of the human body can be predicted through the feedback of human step frequency signals. The sensor location and the human-computer interaction interface set by programming language are shown in Fig. 6(d) and (e), which can be used to monitor the position of force (Supporting Information, Movie S-III).

Supplementary material related to this article can be found online at doi:10.1016/j.nanoen.2023.108697.

Further, the output performance of the device is used to evaluate the movement condition, including slow walking, fast walking, jogging and fast running. To evaluate the applying effect, we conduct a series of experiments by testing four kinds of human movements, such as slow walking, fast walking, jogging and fast running. The monitoring of the exercise experiment is done on a treadmill by the subjects wearing smart sole with integrated sensing functions.

Step frequency is often affected by human body differences. The slow walking of normal adults is 60–80 steps/min, the fast walking is 100–120 steps/min, the jogging is 120–140 steps/min, and the fast running is 180–600 steps/min. Signals from the Miura-ori metamaterials sensors are recorded for 8 s to obtain data sets. The output characteristics of the human body are tested by the triboelectric-piezoelectric sensor as shown in Fig. 6(f). It can be seen from the figure that the frequency of slow walking, fast walking, jogging and fast running is 60 steps/min, 165 steps/min, 180 steps/min, and 525 steps/min. And the output voltages are 142 V, 165 V, 178 V and 207 V for slow walking, fast walking, jogging and fast running. Of the four human movements, the voltage during fast running is the highest because the output voltage is related to the change in the separation distance of the friction layer. When running, the upper and lower friction layer is subjected to greater pendulum force than slow walking, resulting in a more drastic change in the separation distance, so the output voltage is larger.

3. Conclusions

Combined with the origami concept, we propose a series of mechanical metamaterials with programmable stiffness and shape. Utilizing SMP, structures with single topology parameters and gradient topology parameters are fabricated by 4D printing technology. Based on SME, the structure can adjust its configuration to another with different topological parameters. Accordingly, its mechanical properties can be switched between structures with different topological parameters, which greatly expands its application range. Experiments indicate that the metamaterials with the same topological parameter obtained by the initial design and after the programming process exhibits similar mechanical properties. Further, we investigate the compression performance of the structure with different topological parameters and analyze the energy absorption properties of each structure. By integrating the TENG and PENG functions into the structure, we explore and find that this class of structures exhibits excellent energy harvesting ability, and proves good robustness under long-time contact. Finally, utilizing M-III-2 with excellent energy absorption capacity, we fabricate a sole, and the gait monitoring function is successfully realized by integrating the sensing and self-powered functions. 4D printing technology has unique advantages in structure fabrication and reprogramming after structure fabrication, which will bring more possibilities for the functional integration and application of TENG.

CRediT authorship contribution statement

Wei Zhao and Nan Li: Conceptualization, Methodology, Wei Zhao, Nan Li, Xu Liu, Chengbin Yue and Chengjun Zeng: Data curation, Writing- Original draft preparation. Wei Zhao, Xu Liu and Nan Li:: Visualization, Investigation. Liwu Liu, Yanju Liu anf Jinsong Leng:Supervision. Wei Zhao and Nan Li, Yanju Liu:Writing- Reviewing and Editing.

Declaration of Competing Interest

The authors declare that they have no known competing financial interests or personal relationships that could have appeared to influence the work reported in this paper.

Data Availability

Data will be made available on request.

Acknowledgment

This work was supported by the National Natural Science Foundation of China (Grant No. 12072094), China Postdoctoral Science Foundation (No. 2022M720962), and Postdoctoral Science Foundation of Heilongjiang Province (No. LBH-Z22114).

Appendix A. Supporting information

Supplementary data associated with this article can be found in the online version at doi:10.1016/j.nanoen.2023.108697.

References

[1] X.L. Yu, J. Zhou, H.Y. Liang, Z.Y. Jiang, L.L. Wu, Mechanical metamaterials associated with stiffness, rigidity and compressibility: a brief review, Prog. Mater. Sci. 94 (2018) 114–173.
[2] S.Y. Li, H.B. Fang, S. Sadeghi, P. Bhovad, K.W. Wang, Architected origami materials: how folding creates sophisticated mechanical properties, Adv. Mater. 31 (5) (2019), 1805282.
[3] A.A. Zadpoor, Mechanical meta-materials, Mater. Horiz. 3 (5) (2016) 371–381.
[4] S.M. Montgomery, X. Kuang, C.D. Armstrong, H.J. Qi, Recent advances in additive manufacturing of active mechanical metamaterials, Curr. Opin. Solid State Mater. Sci. 24 (5) (2020), 100869.
[5] W. Zhao, N. Li, L.W. Liu, J.S. Leng, Y.J. Liu, Origami derived self assembly stents fabricated via 4D printing, Compos. Strucutres 293 (2022), 115669.
[6] W. Zhao, C.B. Yue, L.W. Liu, J.S. Leng, Y.J. Liu, Mechanical behavior analyses of 4D printed metamaterials structures with excellent energy absorption ability, Compos. Struct. 304 (2023), 116360.
[7] X.Z. Xin, L.W. Liu, Y.J. Liu, J.S. Leng, 4D printing auxetic metamaterials with tunable, programmable, and reconfigurable mechanical properties, Adv. Funct. Mater. 30 (2020), 2004226.

[8] F. Pan, Y.L. Li, Z.Y. Li, J.L. Yang, B. Liu, Y.L. Chen, 3D pixel mechanical metamaterials, Adv. Mater. 31 (2019), 1900548.
[9] X. Ni, X. Guo, J. Li, Y. Huang, Y. Zhang, J.A. Rogers, 2D mechanical metamaterials with widely tunable unusual modes of thermal expansion, Adv. Mater. 31 (2019), 1905405.
[10] J. Liu, Y. Zhang, Soft network materials with isotropic negative Poisson's ratios over large strains, Soft Matter 14 (2018) 693–703.
[11] Q.L. Zeng, S.Y. Duan, Z.A. Zhao, P.D. Wang, H.S.Lei Inverse, design of energy-absorbing metamaterials by topology optimization, Adv. Sci. 10 (4) (2022), 2204977.
[12] T. van Manen, S. Janbaz, K.M.B. Jansen, A.A. Zadpoor, 4D printing of reconfigurable metamaterials and devices, Commun. Mater. 2 (2021) 56.
[13] Z.Q. Meng, M.C. Liu, H.J. Yan, M.Genin Guy, C.Q. Chen, Deployable mechanical metamaterials with multistep programmable transformation, Sci. Adv. 8 (2022) eabn5460.
[14] K. Bertoldi, V. Vitelli, J. Christensen, M. Van Hecke, Flexible mechanical metamaterials, Nat. Rev. Mater. 2 (11) (2017) 17066.
[15] B.K. Ashley, M.S. Brown, Y. Park, S. Kuan, A. Koh, Skin-inspired, open mesh electrochemical sensors for lactate and oxygen monitoring, Biosens. Bioelectron. 132 (2019) 343–351.
[16] J. Wong, A.T. Gong, P.A. Defnet, L. Meabe, B. Beauchamp, R.M. Sweet, H. Sardon, C.L. Cobb, A. Nelson, 3D printing ionogel auxetic frameworks for stretchable sensors, Adv. Mater. Technol. 4 (9) (2019), 1900452.
[17] J. Shintake, T. Nagai, K. Ogishima, AI Sensitivity improvement of highly stretchable capacitive strain sensors by hierarchical auxetic structures, Front. Robot. AI 6 (2019) 127.
[18] J. Kim, H. Hegde, H.Y. Kim, C. Lee, Spindle vibration mitigation utilizing additively manufactured auxetic materials, J. Manuf. Process 73 (2022) 633–641.
[19] T. Frenzel, C. Findeisen, M. Kadic, P. Gumbsch, M. Wegener, Tailored buckling microlattices as reusable light-weight shock absorbers, Adv. Mater. 28 (28) (2016) 5865–5870.
[20] N. San, Ha, T.M. Pham, T.T. Tran, H. Hao, G. Lu, Mechanical properties and energy absorption of bio-inspired hierarchical circular honeycomb, Compos. Part B: Eng. 236 (2022), 109818.
[21] J.W. Boley, W.M. Van Rees, C. Lissandrello, M.N. Horenstein, R.L. Truby, A. Kotikian, J.A. Lewis, L. Mahadevan, Shape-shifting structured lattices via multimaterial 4D printing, Proc. Natl. Acad. Sci. USA 116 (42) (2019) 20856–20862.
[22] L.C. Wang, W.L. Song, Y.J. Zhang, M.J. Qu, Z. Zhao, M.J. Chen, Y.Z. Yang, H. S. Chen, D.N. Fang, Active reconfigurable tristable square-twist origami, Adv. Funct. Mater. 30 (13) (2020), 1909087.
[23] Z. Wang, L. Jing, K. Yao, Y. Yang, B. Zheng, C.M. Soukoulis, H. Chen, Y. Liu, Origami-based reconfigurable metamaterials for tunable chirality, Adv. Mater. 29 (27) (2017), 1700412.
[24] X.L. Zhou, L.Q. Ren, Z.Y. Song, G.W. Li, J.F. Zhang, B.Q. Li, Q. Wu, W.X. Li, L. Ren, Q.P. Liu, Advances in 3D/4D printing of mechanical metamaterials: from manufacturing to applications, Compos. Part B: Eng. 254 (2023), 110585.
[25] Y. Chen, H.J. Feng, J.Y. Ma, R. Peng, Z. You, Symmetric waterbomb origami, Proc. R. Soc. a-Math. Phys. Eng. Sci. 472 (2190) (2016).
[26] S.C. Liu, W.L. Lv, Y. Chen, G.X. Lu, Deployable prismatic structures with rigid origami patterns, J. Mech. Robot. -Trans. ASME 8 (3) (2016), 031002.
[27] Z.R. Zhai, L.L. Wu, H.Q. Jiang, Mechanical metamaterials based on origami and kirigami, Appl. Phys. Rev. 8 (2021), 041319.
[28] M. Schenk, S.D. Guest, Geometry of miura-folded metamaterials, Proc. Natl. Acad. Sci. 110 (9) (2013) 3276–3281.
[29] S. Sadeghi, S. Li, Fluidic origami cellular structure with asymmetric quasi-zero stiffness for low-frequency vibration isolation, Smart Mater. Struct. 28 (6) (2019) 65006.
[30] J.A. Harris, G.J. McShane, Metallic stacked origami cellular materials: additive manufacturing, properties, and modelling, Int. J. Solids Struct. 185 (2020) 448–466.
[31] S. Kamrava, D. Mousanezhad, H. Ebrahimi, R. Ghosh, A. Vaziri, Origami-based cellular metamaterial with auxetic, bistable, and self-locking properties, Sci. Rep. 7 (2017) 46046.
[32] H. Zhang, J. Wu, D.N. Fang, Y.H. Zhang, Hierarchical mechanical metamaterials built with scalable tristable elements for ternary logic operation and amplitude modulation, Sci. Adv. 7 (9) (2021) eabf1966.
[33] N. Yang, J.L. Silverberg, Decoupling local mechanics from large-scale structure in modular metamaterials, Proc. Natl. Acad. Sci. USA 114 (14) (2017) 3590–3595.
[34] J.X. Qi, Z.H. Chen, P. Jiang, W.X. Hu, Y.H. Wang, Z.A. Zhao, X.F. Cao, S.S. Zhang, R. Tao, Y. Li, D.N. Fang, Recent Progress in active mechanical metamaterials and construction principles, Adv. Sci. 9 (2022), 2102662.
[35] Z.R. Zhai, Y. Wang, H.Q. Jiang, Origami-inspired, on-demand deployable and collapsible mechanical metamaterials with tunable stiffness, Proc. Natl. Acad. Sci. USA 115 (9) (2018) 2032–2037.
[36] J. Zhang, D. Karagiozova, Z. You, Y. Chen, G. Lu, Quasi-static large deformation compressive behaviour of origami-based metamaterials, Int. J. Mech. Sci. 153 (2019) 194–207.
[37] H.G. Kim, S. Hajra, D. Oh, N. Kim, H.J. Kim, Additive manufacturing of high-performance carbon-composites: An integrated multi-axis pressure and temperature monitoring sensor, Compos. Part B-Eng. 222 (2021), 109079.
[38] M.A. Parvez Mahmud, A. Zolfagharian, S. Gharaie, A. Kaynak, S.H. Farjana, A. V. Ellis, J. Chen, A.Z. Kouzani, 3D-printed triboelectric nanogenerators: state of the art, applications, and challenges, Adv. Energy Sustain. Res. 2 (3) (2021), 2000045.
[39] J.X. Wang, X. Liu, Q.S. Yang, R. Tao, Y. Li, L.H. Ma, A novel programmable composite metamaterial with tunable Poisson's ratio and bandgap based on multi-stable switching, Compos. Sci. Technol. 219 (2022), 109245.
[40] X. Liu, Y.Z. Liu, T.H. Cheng, Y.F. Gao, Z.Q. Yang, A high performing piezoelectric and triboelectric nanogenerator based on a large deformation of the novel lantern-shaped structure, Nano Energy 92 (2022), 106699.
[41] D. Liu, C.Y. Li, P.F. Chen, X. Zhao, W. Tang, Z.L. Wang, Sustainable long-term and wide-area environment monitoring network based on distributed self-powered wireless sensing nodes Advanced Energy Materials 13(2) (2022).
[42] S.C. Yao, M.J. Zheng, Z. Wang, Y.C. Zhao, S.B. Wang, Z.R. Liu, Z. Li, Y.Q. Guan, Z. L. Wang, L.L. Li, Self-powered, implantable, and wirelessly controlled NO generation system for intracranial neuroglioma therapy, Adv. Mater. 34 (50) (2022).
[43] S. Hajra, J. Panda, J. Swain, H.G. Kim, M. Sahu, M.K. Rana, R. Samantaray, H. J. Kim, R. Sahu, "Triazine skeletal covalent organic frameworks: a versatile highly positive surface potential triboelectric layer for energy harvesting and self-powered applications,", Nano Energy 101 (2022), 107260.
[44] S. Kamrava, D. Mousanezhad, H. Ebrahimi, R. Ghosh, A. Vaziri, Origami-based cellular metamaterial with auxetic, bistable, and self-locking properties, Sci. Rep. 7 (1) (2017) 46046.
[45] S. Yang, Y. He, J.S. Leng, Shape memory poly (ether ether ketone)s with tunable chain stiffness, mechanical strength and high transition temperatures, Int. J. Smart Nano Mater. 13 (1) (2022) 1–16.
[46] W. Zhao, J. Zhu, L.W. Liu, Y.J. Liu, J.S. Leng, A bio-inspired 3D metamaterials with chirality and anti-chirality topology fabricated by 4D printing, Int. J. Smart Nano Mater. 14 (1) (2023) 1–20.
[47] W. Zhao, F.H. Zhang, J.S. Leng, Y.J. Liu, Personalized 4D printing of bioinspired tracheal scaffold concept based on magnetic stimulated shape memory composites, Compos. Sci. Technol. 184 (2019), 107866.